Volume 25
Number 22
14 June 2023
Pages 3247–3348

CrystEngComm

rsc.li/crystengcomm

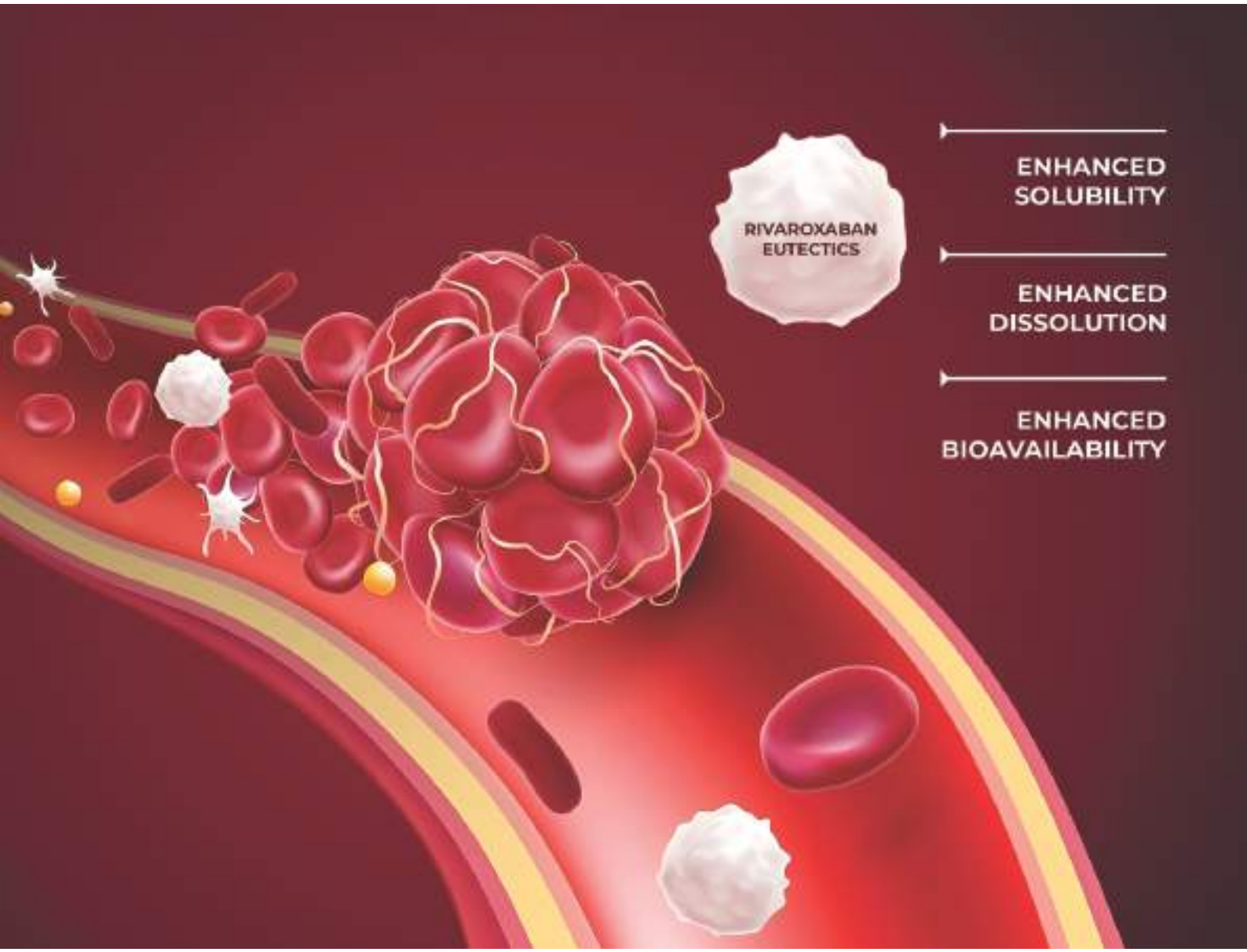

ISSN 1466-8033

ROYAL SOCIETY
OF CHEMISTRY

PAPER
Rajesh G. Gonnade *et al.*
Rivaroxaban eutectics with improved solubility, dissolution rates, bioavailability and stability

CrystEngComm

ROYAL SOCIETY OF CHEMISTRY

PAPER

View Article Online
View Journal | View Issue

Cite this: *CrystEngComm*, 2023, **25**, 3253

Rivaroxaban eutectics with improved solubility, dissolution rates, bioavailability and stability†

Parth S. Shaligram,[ab] Christy P. George,[ac] Himanshu Sharma,[ac] Kakasaheb R. Mahadik,[b] Sharvil Patil,[b] Kumar Vanka,[ac] S. Arulmozhi*[b] and Rajesh G. Gonnade*[ac]

Rivaroxaban (RXB) is a direct factor Xa inhibitor used for the treatment of deep vein thrombosis (DVT, a blood clot in the leg) and pulmonary embolism (PE, a blood clot in the lung) and to prevent blood clots in atrial fibrillation following hip or knee surgery. However, RXB suffers from poor solubility that hinders its broader application. Although its cocrystals are reported for solubility enhancement, the methodology used to prepare multi-component crystals is complex. Also, it uses hazardous solvents to develop cocrystals. We have prepared eutectics of RXB with caffeic acid (CAA), coumaric acid (CA), fumaric acid (FA), succinic acid (SA), mandelic acid (MA) and trimesic acid (TA) and analyzed them using hot stage microscopy (HSM), differential scanning calorimetry (DSC), powder X-ray diffraction (PXRD), and fourier transform infrared spectroscopy (FTIR) techniques. The saturation solubility and dissolution rate profiles were also obtained to investigate the effect of eutectics on these parameters. Amongst all the coformers tested, coformers CAA, CA, and FA showed significant enhancement in the solubility of RXB. The powder dissolution rate of the eutectics showed considerable enhancement compared to that of RXB. *In vivo* pharmacokinetic study was carried out for RXB–CAA, RXB–CA and RXB–FA in rats and compared with RXB, which showed 1.5 and 1.4 times enhancement in relative bioavailability for RXB–CAA and RXB–CA, respectively. Stability studies were carried out as per ICH guidelines for all the eutectics, which revealed excellent stability over six months under accelerated (40 °C and 75%) conditions and twelve months under long-term (30 °C and 60% RH) conditions. The DFT studies carried out using the B3LYP/TZVP level of theory revealed higher Gibbs free interaction energy (ΔG_{int}) for homosynthons (drug···drug and coformer···coformer) than heterosynthons (drug···coformer).

Received 16th March 2023,
Accepted 24th April 2023

DOI: 10.1039/d3ce00261f

rsc.li/crystengcomm

Introduction

Direct factor Xa inhibitors are known to inhibit factor Xa, the factor responsible for converting prothrombin to thrombin, which leads to the formation of a blood clot.[1,2] Factor Xa inhibitors are active against both free factor Xa and the prothrombinase complex of factor Xa. These inhibitors are the most commonly used medications to manage blood clots (deep vein thrombosis) and pulmonary embolism (PE). Rivaroxaban ((*S*)-5-chloro-*N*-({2-oxo-3-[4-(3-oxomorpholin-4-yl)phenyl]oxazolidin-5-yl}methyl)thiophene-2-carboxamide) (Fig. 1) is used to prevent blood clots after knee and hip surgeries and in patients with active cancer, wherein the

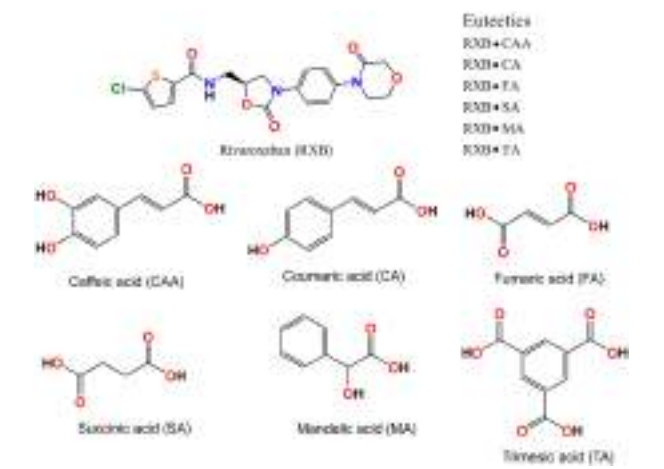

Fig. 1 Molecular structure of rivaroxaban and coformers.

[a] *Physical and Materials Chemistry Division, CSIR-National Chemical Laboratory, Dr. Homi Bhabha Road, Pashan, Pune, 411008 India.*
E-mail: rg.gonnade@ncl.res.in; Fax: +91 20 25902642; Tel: +91 20 25902225
[b] *Poona College of Pharmacy, Bharati Vidyapeeth Deemed to be University, Erandwane, Pune-411038, Maharashtra, India*
[c] *Academy of Scientific and Innovative Research (AcSIR), Sector 19, Kamla Nehru Nagar, Ghaziabad, Uttar Pradesh 201002, India*

† Electronic supplementary information (ESI) available: PXRD patterns, DSC data, FTIR profiles, HSM and SEM photomicrographs, binary phase diagram, solubility data, dissolution rate and PK studies, DFT results, *etc.* See DOI: https://doi.org/10.1039/d3ce00261f

chances of venous thromboembolism are high. It was approved by the US Food and Drug Administration (FDA) for the treatment of deep vein thrombosis (DVT) and pulmonary embolism (PE) and to prevent blood clots in atrial fibrillation following hip or knee surgery, to reduce the risk of recurrence of DVT/PE.[3] Rivaroxaban (RXB) is also used along with many chemotherapeutic agents.[4] The patent WO2007039132 has reported the crystalline forms I, II, and III, the amorphous form, the hydrate, the NMP (*N*-methyl-2-pyrrolidon) solvate and the THF (tetrahydrofuran) clathrate of RXB.[5] RXB, a BCS class II drug, suffers from the drawback of poor aqueous solubility, affecting its bioavailability.[6] Moreover, it is practically insoluble in most industrial solvents such as ethanol, methanol, isopropyl alcohol, *etc.* The marketed formulation of RXB is the Xarelto tablet with oral dosages of 10 mg, 15 mg, and 20 mg potencies. Formulation scientists worldwide are working to tackle the problems of aqueous solubility, which would improve its bioavailability. Therefore, efforts have been made to develop alternative crystalline phases of RXB to enhance its physicochemical properties, positively impacting its therapeutic efficacy. This is usually achieved by developing novel solid formulations, including solid dispersions, micronization, amorphous formulation, microemulsion, nano-formulation, *etc.* An alternative approach that has had incredible implications in drug delivery in the last two decades is to explore novel crystalline phases of APIs like polymorphs and crystals, including cocrystals, salts, eutectics, solid solutions and hydrates.[7,8] The new formulations can enhance the physicochemical, mechanical, and biopharmaceutical properties of active pharmaceutical ingredients (APIs) like solubility, stability, hygroscopicity, crystallinity, compressibility, compactibility, bioavailability, permeability, *etc.*, and hence it may aid in improving their therapeutic efficacy. Two cocrystals of RXB with malonic acid[9,10] and oxalic acid[11] used for aqueous solubility enhancement have been reported. However, corrosive solvents like 2,2,2-trifluoroethanol are used to prepare these cocrystals. Additionally, the method of development of these cocrystals is also very tedious. Therefore, we have attempted to develop novel solid formulations, eutectics[12–14] of RXB, to resolve its poor aqueous solubility in the present work. Vasconcelos *et al.* in 2007 classified eutectics as "first-generation solid dispersions," wherein[7,15] an active pharmaceutical ingredient (API) forms a complex with highly water-soluble moieties. Hence, such mixtures show faster release rates and higher bioavailability than pure drugs. Furthermore, it has been observed that the combination of highly water-soluble compounds with APIs enhances the wettability and bioavailability of the corresponding medications.[7,8] Similarly, the amorphous form of an API is a "latter-generation solid dispersion,"[16] wherein the amorphous form of the drug shows higher dissolution rates. However, the major drawback of the amorphous solid phase is its poor physical stability and inclination toward crystallization. An amorphous API is generally susceptible to recrystallization, structural denaturation, and degradation because of high free energy.[17] The two components in a binary eutectic mixture do not interact with each other to form a new compound, but these components, when mixed at particular molar ratios, inhibit the crystallization process resulting in the formation of a new system with a relatively lower melting point than the original pure components.[7,18–20] In a eutectic, API exists in crystalline form, eliminating the drawbacks associated with amorphous systems. Therefore, currently, pharmaceutical scientists are giving special attention to this novel approach to tune the physicochemical and biopharmaceutical properties of a drug substance.

The literature presents a lacuna in developing eutectic mixtures of RXB to improve its aqueous solubility. Thus, this study aimed to prepare and screen possible eutectics of RXB using acidic moieties, namely, caffeic acid (CAA), coumaric acid (CA), fumaric acid (FA), succinic acid (SA), mandelic acid (MA), and trimesic acid (TA) (Fig. 1). Acidic coformers were chosen for eutectic development as RXB comprises several hydrogen bonding acceptor functional groups, including an amine donor group. The resulting eutectics were analysed using powder X-ray diffraction (PXRD), differential scanning calorimetry (DSC), hot stage microscopy (HSM) and infrared spectroscopy (IR).[21] Further, saturation solubility and powder dissolution studies were performed to monitor the dissolution properties of the prepared eutectics. Though improvement in the dissolution properties is one of the major contributing factors which can lead to improved bioavailability, it is not the sole factor deciding it. There are equally contributing factors like the absorption rate constant (k_a), intestinal transit time, drug metabolism, *etc.* Solid state alterations can affect the permeability of drugs across the biomembrane, which can interplay with the dissolution and can result in a positive or negative shift in the overall bioavailability. To clearly elicit the translation pattern of the *in vitro* dissolution to the *in vivo* conditions, pharmacokinetic (PK) studies were carried out by administering RXB, RXB–CA, RXB–CAA, and RXB–FA eutectics in Wistar rats and their plasma concentration–time profiles were compared with the dissolution pattern. To predict the favourable synthons (homo or hetero) between RXB and the acidic coformers, a DFT study was carried out at the B3LYP/TZVP level of theory.

Experimental

Materials and methods

RXB was a generous gift from Alkem Pharma, India. Caffeic acid and coumaric acid were purchased from HiMedia, Mumbai. Fumaric acid, trimesic acid and mandelic acid were purchased from Aldrich Chemistry, Mumbai. Succinic acid was purchased from Sisco Research Laboratories Pvt. Ltd., Mumbai, India. All other chemicals and solvents used were of analytical grade. Distilled water was generated from a Millipore Direct-Q ultra-pure water system (Merck Millipore, India).

Synthesis of eutectics

The liquid-assisted grinding (LAG) method[16] was utilized to prepare the eutectics of RXB. Various acidic moieties were chosen as coformers.[22] Each eutectic was developed by grinding the RXB and the corresponding acids using a mortar and pestle. A mixture of ethanol and acetone (1 : 1 v/v) was added as a catalyst and/or lubricant.[17] The mortar and pestle generated the energy required to cause the intermolecular interaction between RXB and the respective acidic moieties.[17] The resultant solids were isolated and subjected to further analysis.

Hot stage microscopy (HSM) studies

The samples, namely, RXB–CAA, RXB–CA, RXB–FA, RXB–SA, RXB–MA and RXB–TA were subjected to hot stage microscopy on a Linkam Scientific Instruments Ltd. (Tadworth, England) instrument equipped with an EHEIM professional 4+ temperature controller and an optical microscope (Leica S8APO) with a Q imaging camera to capture images. The sample was focused under the microscope at 10× zoom with photos collected after specific intervals during the heating process wherein the samples were heated from 50 °C to 100 °C at 10 °C min^{-1}, followed by heating to 250 °C at 5 °C min^{-1}, and finally to 300 °C at 10 °C min^{-1}.

Binary phase diagram

The phase diagram study of RXB–CAA, RXB–CA, RXB–FA, RXB–SA, RXB–MA and RXB–TA samples was carried out with varying mole fractions and the diagrams were plotted to confirm the exact molar ratio required to form a eutectic.[23] Mixtures of varying mole fractions from 1 : 1 to 1 : 9 were made for all six potential candidates by grinding the sample using a mortar and pestle. DSC analysis of all the mixtures was performed carefully to monitor their melting pattern and determine their exact molar ratios.

Differential scanning calorimetry (DSC) analysis

DSC was conducted on a Mettler Toledo DSC822e instrument by measuring the enthalpy change. The system was calibrated with indium before the analysis.[24,25] 2 mg samples were accurately weighed into an aluminium pan and sealed properly. An empty pan was locked similarly and used as a reference. The reference and RXB–CAA (1 : 2), RXB–CA (1 : 2), RXB–FA (1 : 2), RXB–SA (1 : 2), and RXB–MA (1 : 4) samples were analyzed between 25 °C and 300 °C. The RXB–TA (1 : 1) sample was analyzed between 25 °C and 400 °C. A heating rate of 10 °C min^{-1} was used to improve the observation accuracy for all thermal events.[20] A nitrogen flow rate of 40 mL min^{-1} was used for each analysis. The DSC melting peak temperatures of the pure RXB and CAA, CA, FA, SA, MA, TA and eutectic mixtures were used to identify the eutectic point. From the DSC analysis, all the measurable melting temperatures were plotted as a function of RXB and the coformers (CAA, CA, FA, SA, MA, and TA) in the respective molar ratios which were confirmed from phase diagram studies.

Powder X-ray diffraction (PXRD) studies

The powder X-ray diffraction (PXRD) patterns of powder samples were recorded on an X'Pert PRO diffractometer system (PANalytical, Almelo, Netherlands) with Cu-Kα radiation. The tube voltage and current were set at 45 kV and 40 mA, respectively. The divergence slit and anti-scattering slit settings were set at 0.48° for the 10 mm sample size diffraction experiment. Each sample was placed in a glass sample holder and continuously scanned between 3.5° and 50° 2θ with a step size of 0.017° and a step time of 25 s per step.[26] The experimental PXRD patterns were refined using X'Pert HighScore software (Malvern Panalytical).

Fourier transform infrared spectroscopy (FTIR)

Infrared spectroscopy was carried out using a JASCO FT/IR-4100 Fourier transform infrared spectrometer. FTIR analysis of RXB, carboxylic acids and all the eutectics was performed in KBr transmittance mode (sample concentration 2 mg in 20 mg of KBr). Scans were recorded over the range of 4000–400 cm^{-1} with a resolution of 4 cm^{-1}. Data were analysed using Spectra Manager software (JASCO).

Saturation solubility studies

RXB, its eutectics and physical mixtures with coformers (CAA, CA, FA, SA, MA and TA) were analyzed for saturation solubility in distilled water. An excess of each sample was added to distilled water. The saturated solutions were stirred for 24 h at room temperature at 500 rpm speed using a Tarson SPINOT digital magnetic stirrer. The concentration of RXB present in the medium was determined by HPLC.

Field emission scanning electron microscopy (FESEM) studies

The size, shape and morphology of the eutectic samples were studied by means of an FEI Nova NANO 450 Quanta 200 3D field emission scanning electron microscope with a field electron gun (FEG). The operating conditions were a 20 kV electron beam and a 10 mm working distance. All the samples to be analyzed using FESEM were initially processed by the LAG method mentioned previously. The samples were sprinkled on a double-sided carbon tape adhered to an aluminium stub. Before imaging, the mounted samples were sputter-coated with a thin layer of gold by using an Emitech sputter coater (POLARON model SC7640). XT Microscope Server Software (FEI, FrameMakerTM) was used for obtaining particle size data from SEM images.

Dissolution studies

Dissolution studies of the drug RXB and its eutectic and physical mixtures were performed using a LabIndia

dissolution apparatus with an autosampler attached to it. Powder samples were ground uniformly (individually for RXB and coformers before making their physical mixtures) and sieved through 100 mesh size sieves to ensure similar particle sizes. Dissolution studies of powders of RXB (15 mg), the optimized eutectics (equivalent to 15 mg RXB) and their physical mixtures (equivalent to 15 mg RXB) were performed in distilled water for 1 hour. The dissolution apparatus USP type II was used. All the dissolution studies were conducted at 36 °C, and the rpm of the paddle was set at 75. Sampling was done using a LabIndia auto sampling assembly. 2 mL of samples was taken at 5 min, 10 min, 15 min, 30 min, 45 min, and 60 min. The samples were analyzed by using HPLC.

HPLC analysis

Plasma concentrations of RXB were determined by extraction of the drug from plasma followed by reversed phase high-performance liquid chromatography (HPLC) with UV detection. Plasma (0.3 mL) from a standard or sample was dispensed into a vial and then 0.3 mL of acetonitrile and 0.025 mL of methanol were added to it. The contents were mixed thoroughly for 3 min and precipitated plasma proteins were separated by centrifugation at 8000 rpm. 5 μL of the clear supernatant layer was injected onto a Waters 515 HPLC with a reversed phase column (250 × 4.6 mm; 5 μm; C18) and eluted at a flow rate of 1.2 mL min^{-1} with acetonitrile/water (55 : 45 v/v). Analyte detection was by UV absorbance at 249 nm and, under these conditions, RXB was eluted with a retention time of 3.2–3.4 min. Assay performance was monitored using quality control samples and chromatographic data were obtained using the Empower 3 software (Waters, USA). Quantification was achieved by reference to a calibration series constructed by adding known amounts of the drug to aliquots of control plasma and extracting these standards alongside each batch of samples.

Pharmacokinetic (bioavailability) studies

Male Wistar rats weighing 250–300 g were fasted for 24 h. The animals were given vehicle (PEG 400), pure drug dispersion and eutectic dispersion, the quantity depending on the body weight of the animal. The animals were anesthetized with xylazine and propofol intraperitoneally. The plasma pharmacokinetics of the RXB eutectics in male rats was carried out by a single oral dose of 10 mg kg^{-1} (equivalent doses) of the eutectics suspended in the vehicle. Equivalent doses of the eutectics and standard rivaroxaban were suspended in 1 mL of diluted PEG 400 and were subsequently administered. Doses were given through an oral gavage syringe and the plasma concentration was estimated by withdrawing blood samples by retro orbital plexus puncture (ROP) at specific intervals of time. At the allotted time 1 mL of blood was collected through retro orbital puncture (ROP). Plasma was separated by centrifuging whole blood at 10 000 rpm at 40 °C for 20 minutes. The specific time points were 5, 30, 55, 90, 180, 200, 360 and 720 minutes. Each group had 3 test groups, *i.e.*, 9 animals (3 × 3 animals), so that blood samples could be withdrawn 4 times from each animal. The plasma concentrations were determined by HPLC. The pharmacokinetic parameters were estimated from the plasma concentration through non-compartmental analysis.

Accelerated stability studies

Accelerated stability studies were performed in a stability chamber (Thermolab Scientific Instruments, Mumbai, India). Th eutectic mixtures were kept in vials with lids open for 6 months. The temperature and relative humidity were set at 40 ± 2 °C and 75 ± 2%, respectively.[18,26] The samples were collected and tested after 6 months using DSC.

Long term stability studies

Long term stability studies were performed in a stability chamber (Thermolab Scientific Instruments, Mumbai, India). The eutectic mixtures were kept in vials with lids open for 12 months. The temperature and relative humidity were set at 30 ± 2 °C and 65 ± 5%, respectively. The samples were collected and tested after 12 months using DSC and PXRD.

DFT studies

All the calculations in this study were performed with density functional theory (DFT), with the aid of the TURBOMOLE 7.5.0 suite of programs,[27–30] using the B3LYP functional[31] and the TZVP basis set for all atoms.[32] The Grimme dispersion correction (D3)[33] was employed to consider long-range interactions. Harmonic frequency calculations were performed for all stationary points to confirm them as minima. Thermal correction and zero-point vibration energies were incorporated into the ΔG values. The Multiwfn (v3.7) program package[34] was used to generate the plots for non-covalent interactions (NCI) and the Visual Molecular Dynamics (VMD) program[35] was employed for visualization. The strength of Van der Waals interactions can be determined by calculating the interaction energy. For a eutectic system, the interaction energy can be obtained by subtracting the total energy of RXB and acids from that of the eutectic complex. Likewise, in the case of dimer formation of any acids or RXB, the interaction energy can be calculated by subtracting the total energy of the monomers from that of the dimer complex. The formula for the calculation of interaction energy is given below:

$$\Delta E(\text{complex}) = E(\text{complex}) - E_1 - E_2$$

wherein ΔE(complex) represents the bonding interaction energy, E(complex) refers to the total energy of the complex (eutectic/dimer), and E_1 and E_2 represent the individual energies of the monomers of RXB and acids, respectively.

Results and discussion

Melting point determination

The melting points of the mixtures were observed along with their components simultaneously using a BUCHI melting point apparatus. It was found that RXB–CAA, RXB–CA, RXB–FA, RXB–SA, RXB–MA and RXB–TA samples required lower temperatures to initiate the melting process (ESI† Table S1), which is one of the characteristic features of eutectics.[7,36] The observed melting was sharp and sudden, which indicates the crystalline nature of the eutectics. Therefore, these 6 samples were further analyzed using the hot melt extrusion technique to better understand their melting process.

Hot stage microscopy (HSM) studies

Hot stage microscopy (HSM) was conducted for visual or physical characterization of the prepared samples.[37] It was observed that the samples started melting at lower temperatures than their individual components. The HSM images show the sharp melting of the mixtures, which means that the crystalline nature[38] of both individual moieties in the mixture is not hampered throughout the preparation. Moreover, Fig. 2 shows incomplete melting of RXB–CAA, RXB–CA, RXB–MA and RXB–TA samples, suggesting incomplete conversion into a eutectic with a leftover/excess of the starting substances. Therefore, a binary phase diagram study of all 6 samples was carried out to prepare eutectics without having any traces of excess components. Thus, the HSM results suggested a possibility of the mixtures being eutectic. To confirm the same, further analysis of these samples was performed.

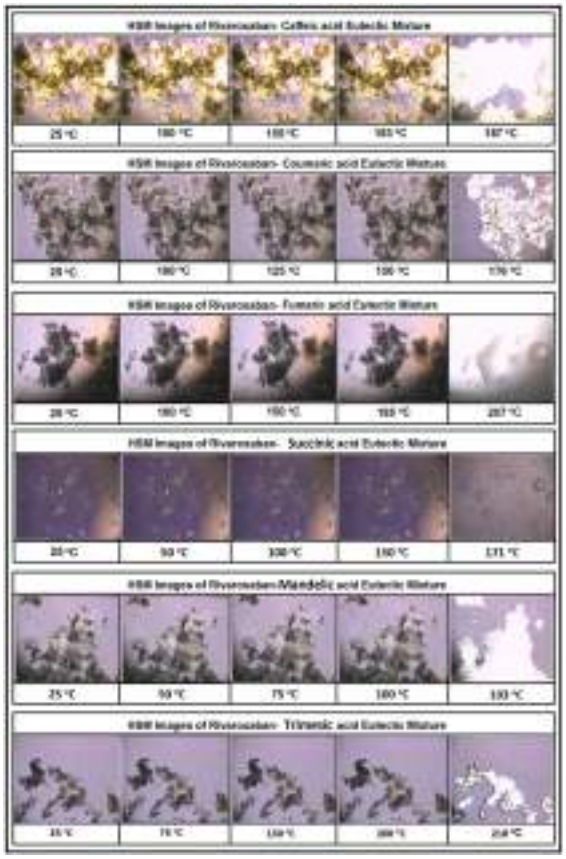

Fig. 2 Photomicrographs of crystalline samples of RXB–CAA, RXB–CA, RXB–FA, RXB–SA, RXB–MA and RXB–TA obtained at different temperatures during hot stage microscopy (HSM) studies.

Binary phase diagram

The construction of a phase diagram is essential to understand the exact composition of the drug and coformers in the eutectic. Solidus and liquidus curves were constructed from the melting temperatures of the binary mixtures in varying molar ratios using DSC studies. The phase diagrams revealed the experimental eutectic point of the binary mixture to be at a 0.33 : 0.66 molar ratio for the RXB–CAA sample (Fig. 3). Also, RXB–CA, RXB–FA and RXB–SA samples showed their eutectic point at a ratio 0.33 : 0.66 (ESI† Fig. S1a–c). On the other hand, the phase diagrams showed the eutectic point at a 0.2 : 0.8 molar ratio for the RXB–MA sample (ESI† Fig. S1d) and at a 0.5 : 0.5 molar ratio for the RXB–TA sample (ESI† Fig. S1e). Therefore, it was concluded that RXB–CAA, RXB–CA, RXB–FA and RXB–SA formed eutectics at a 1 : 2 molar ratio, whereas RXB–MA and RXB–TA formed eutectics at 1 : 4 and 1 : 1 molar ratios, respectively.

Differential scanning calorimetry (DSC) analysis

DSC analysis was carried out to determine the melting point as well as to study the possible structural phase transition during the melting of RXB, all pure acid moieties, and the prepared eutectics.[39] The pristine RXB melted at 231.5 °C (blue), whereas caffeic acid had a melting endotherm at 225 °C (red).

The RXB–CAA (1 : 2) eutectic melted completely at 186 °C (black), which is significantly well below the melting temperatures of RXB and caffeic acid (Fig. 4). Similar results

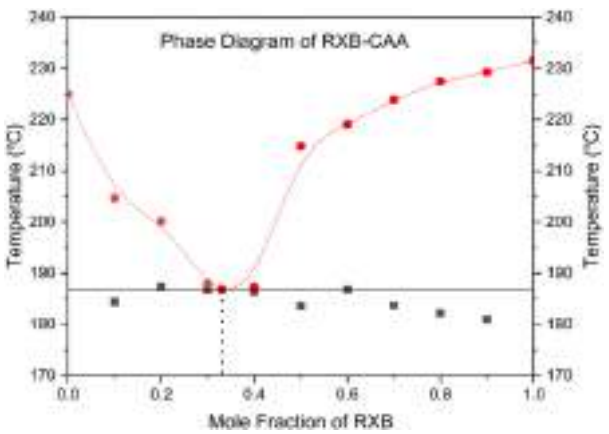

Fig. 3 Phase diagram study of RXB–CAA. The temperature *vs.* mole fraction of RXB plot indicates the eutectic point at a ratio 0.33 : 0.66, *i.e.*, 1 : 2.

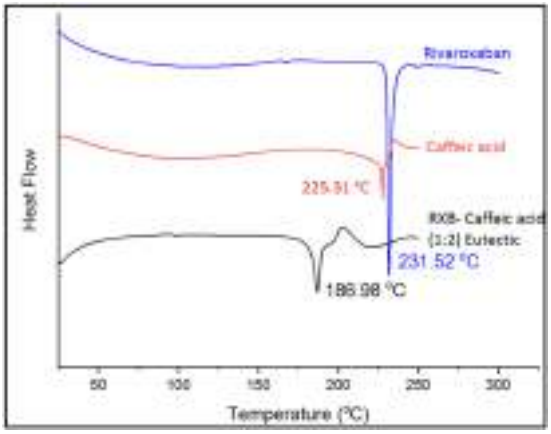

Fig. 4 DSC thermograms of RXB, CA, and RXB–CA (1 : 2).

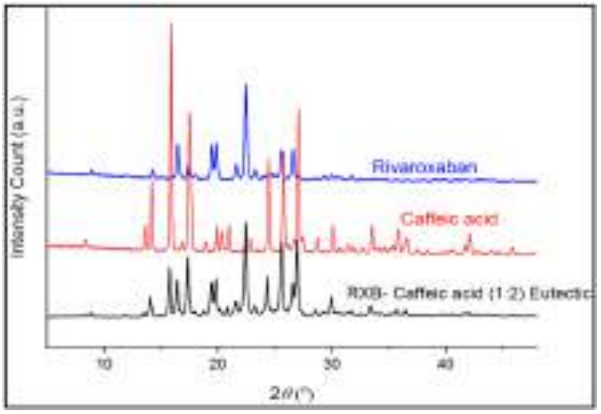

Fig. 5 PXRD profiles of RXB, CAA, and RXB–CAA (1 : 2).

were observed in the case of RXB–CA (1 : 2), RXB–FA (1 : 2), RXB–SA (1 : 2), RXB–MA (1 : 4) and RXB–TA (1 : 1) where a single melting endotherm was observed well below the melting temperatures of RXB and its respective coformers. (ESI† Fig. S2a–e).

All the prepared eutectics RXB–CAA (1 : 2), RXB–CA (1 : 2), RXB–FA (1 : 2), RXB–SA (1 : 2), RXB–MA (1 : 4), and RXB–TA (1 : 1) exhibited melting at temperatures lower than those of their components, confirming their eutectic nature,[40] supplemented by the observations from HSM analysis. Further, the sharp melting endotherms confirmed their crystalline nature. Additionally, the eutectics lacked any residual components and did not display any phase transition during heating. This indicates that RXB–CAA, RXB–CA, RXB–FA and RXB–SA form eutectics in a stoichiometric molar ratio of 1 : 2. In contrast, RXB–MA and RXB–TA form eutectics in stoichiometric ratios of 1 : 4 and 1 : 1, respectively, which supports the results obtained from phase diagram studies.

Powder X-ray diffraction (PXRD) studies

The PXRD profiles of the polymorphs are generally different and so are the PXRD patterns of the cocrystal and its components.[41] Conversely, the PXRD profile of the eutectics shows sharp peaks of individual components, the API, and the coformer, confirming their crystalline nature. The diffractograms of all the eutectics revealed the presence of diffraction peaks of RXB and the corresponding acid. The characteristic diffraction peaks of RXB were observed at 2θ values of 16.25°, 19.89°, 22.5°, 25.48° and 26.96°. Additionally, characteristic 2θ diffraction peaks for CAA were observed at 14.12°, 16.01°, 17.51°, 23.94°, 26.02° and 27.35°. The PXRD pattern of RXB–CAA (1 : 2) showed all the characteristic peaks of RXB and CAA with a minor change in 2θ values at 14.12°, 16.01°, 16.25°, 17.51°, 19.89°, 22.5°, 23.94°, 25.48°, 26.02° and 26.96° (Fig. 5). It shows that RXB–CAA (1 : 2) is a eutectic. Similar results were obtained from the diffractograms of RXB–CA (1 : 2), RXB–FA (1 : 2), RXB–SA (1 : 2), RXB–MA (1 : 4) and RXB–TA (1 : 1) where retention of all the characteristic peaks of RXB and the corresponding coformers was seen with minute changes in 2θ values (ESI† Fig. S3a–e). This also ruled out the possibility of the formation of cocrystals of RXB with selected coformers.

Fourier transform infrared (FTIR) spectroscopy studies

The intermolecular interactions amongst molecules could be analysed using infrared (IR) spectroscopy owing to its ability to record the changes in vibrational modes of covalent bonds. IR spectroscopy of the eutectics was performed to check if any interaction between RXB and coformers exists.[23] RXB showed characteristic bands at 3366 cm^{-1} for the amine group, at 1737 cm^{-1} for the –C═O group, and at 832 cm^{-1} for the C–Cl group. CAA showed characteristic peaks at 3400–3444 cm^{-1} for the –OH group, at 1418 cm^{-1} for OH bending in carboxylic acid, and at 1746 cm^{-1} for C═O stretching in the carboxylic acid group. Meanwhile, the FTIR analysis of the eutectic RXB–CAA (1 : 2) showed vibrational frequencies at 3368 cm^{-1}, 1738 cm^{-1}, 813 cm^{-1}, 3438 cm^{-1}, 1417 cm^{-1} and 1738 cm^{-1}, similar to those of the individual components RXB and CAA (Fig. 6). Similarly, the vibrational frequencies observed in the FTIR spectra of other eutectics, namely, RXB–

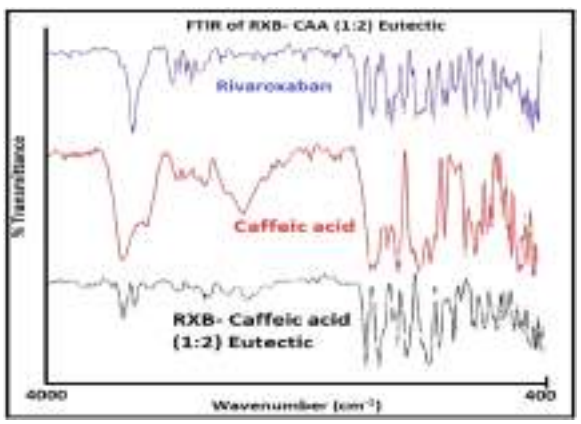

Fig. 6 FTIR spectra of RXB, CAA, and RXB–CAA (1 : 2).

CA (1 : 2), RXB–FA (1 : 2), RXB–SA (1 : 2), RXB–MA (1 : 4) and RXB–TA (1 : 1) were similar to those of their components with minute shifts (ESI† Table S2 and Fig. S4a–e). The FTIR studies showed minute shifts in their vibrational frequencies. The differences in their frequencies are too small to conclude any structural changes and the identity of the individual components remained intact.

Saturation solubility studies

RXB shows a pH-independent solubility; therefore, the saturation solubility of RXB, the eutectics and physical mixtures of RXB and coformer acids was determined in distilled water.[42] The eutectics showed a slight increase in saturation solubility as compared to RXB in all the cases. Among them, RXB–CAA (1 : 2), RXB–CA (1 : 2) and RXB–FA (1 : 2) showed comparatively higher solubility. Also, the coformers CAA, CA and FA contain conjugated carboxylic acid groups absent in SA, MA and TA (Fig. 1). On the other hand, the solubility of physical mixtures of RXB and coformer acids remained similar to that of pristine RXB. (ESI† Table S3). Under physiological conditions, the dissolution rate plays an important role in determining the bioavailability of a drug. Since RXB has a $t_{1/2}$ value of 2 hours the drug dissolution rate is a much more important parameter to analyze. Therefore, dissolution studies were carried out on selected eutectics that showed better solubility, namely, RXB–CAA, RXB–CA and RXB–FA.

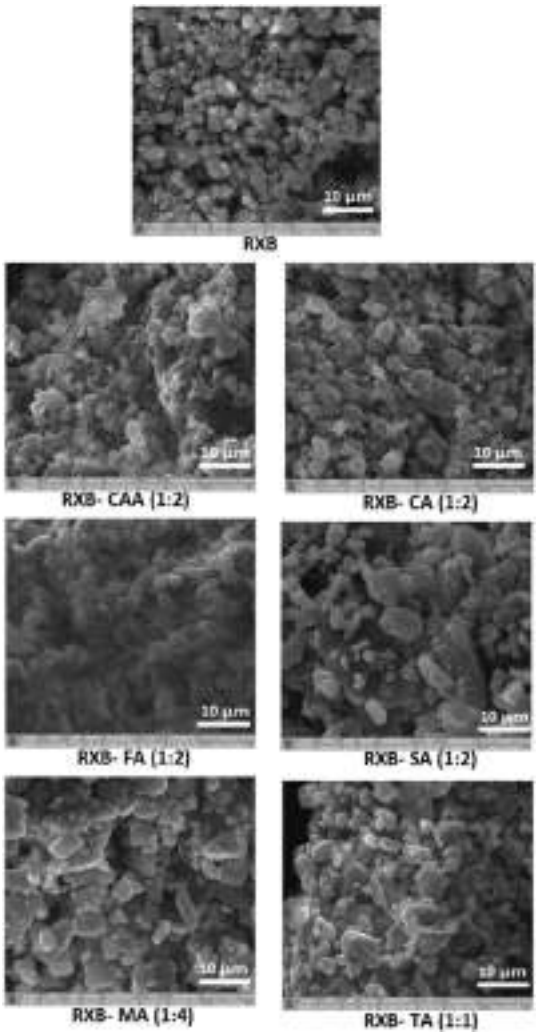

Fig. 7 SEM images of RXB–CAA (1 : 2), RXB–CA (1 : 2), RXB–FA (1 : 2), RXB–SA (1 : 2), RXB–MA (1 : 4) and RXB–TA (1 : 1) under a 20 kV electron beam and a 10 mm working distance.

Field emission scanning electron microscopy (FESEM) studies

The external morphology of polycrystalline samples of RXB, RXB–CAA (1 : 2), RXB–CA (1 : 2), RXB–FA (1 : 2), RXB–SA (1 : 2), RXB–MA (1 : 4) and RXB–TA (1 : 1) was examined by scanning electron microscopy (SEM) (Fig. 7). RXB powder particles were found to be regular in shape and size as the API was micronized fine powder from the manufacturer. Most of the RXB particles were in the range of 2–3 μm. It was observed from the SEM images that the crystal engineering process to obtain eutectics of RXB has considerably changed the original size and shape of the RXB polycrystalline material. The crystals of RXB–CAA (1 : 2), RXB–CA (1 : 2), RXB–FA (1 : 2), RXB–SA (1 : 2), and RXB–MA (1 : 4) and the liquid assisted grinding (LAG) method generally results in polydispersity of the particles.[16] As eutectics have higher surface energy, the aggregation tendency is also high. It was also found that the mean particle sizes of eutectics RXB–CAA (1 : 2), RXB–CA (1 : 2) and RXB–FA (1 : 2) were 1.21 μm, 2.20 μm and 2.68 μm, respectively. They are comparatively smaller than RXB–SA (1 : 2), RXB–MA (1 : 4) and RXB–TA (1 : 1), having mean particle sizes of 5.22 μm, 5.15 μm and 3.67 μm, respectively. The higher solubility for RXB–CAA (1 : 2), RXB–CA (1 : 2) and RXB–FA (1 : 2) eutectics could be due to their small particle size

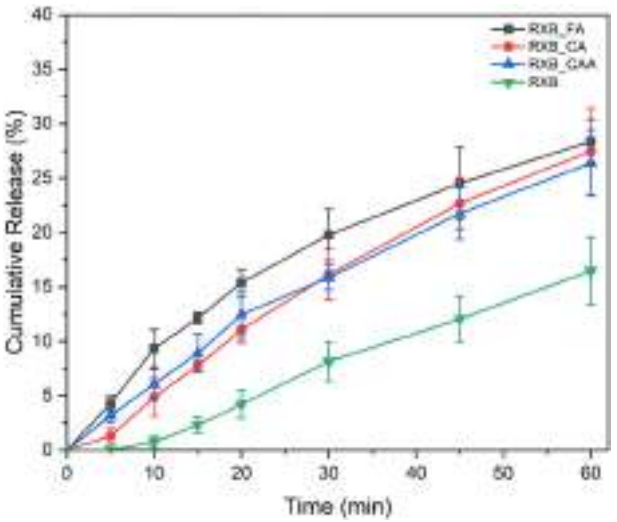

Fig. 8 Tablet dissolution profiles of RXB alone, RXB–CAA (1 : 2), RXB–CA (1 : 2) and RXB–FA (1 : 2) in distilled water.

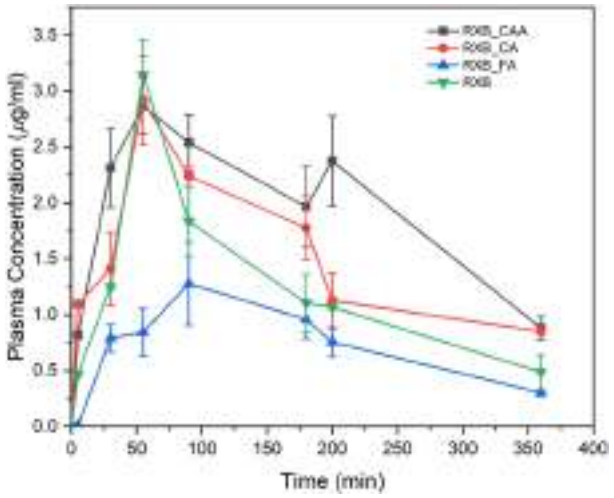

Fig. 9 Plasma concentration *versus* time plot for rivaroxaban (pure drug), RXB–CAA, RXB–CA and RXB–FA.

and larger surface area. Also, SEM images of RXB–SA (1 : 2), RXB–MA (1 : 4) and RXB–TA (1 : 1) showed more agglomeration, which might have resulted in their low solubility.

Dissolution studies

A dissolution study was performed to analyze the dissolution pattern of the eutectics. The rivaroxaban marketed tablet is an immediate-release tablet; therefore, a dissolution study for 1 h was performed in distilled water as a dissolution medium.[43,44] RXB and selected eutectic powders equivalent to 15 mg of the drug were used for the dissolution study. RXB showed a cumulative release of 16%; also, the dissolution study for the physical mixtures showed no significant change in the dissolution properties compared to pure rivaroxaban. (ESI† Table S4), whereas RXB–CAA, RXB–CA and RXB–FA showed enhanced cumulative release values of 26%, 27% and 28%, respectively (Fig. 8). All the three eutectics showed a significant increase in their dissolution rates as compared to pure RXB powder. It is observed that the cumulative release values at 60 minutes are comparatively similar for RXB–CAA, RXB–CA and RXB–FA (ESI† Table S5). Initially RXB–FA shows a higher release which eventually plateaus near the 60 min of the dissolution study. RXB–CAA and RXB–CA showed similar release profiles throughout the study.

Pharmacokinetic (bioavailability) studies

The plasma profiles of RXB and three eutectics, namely, RXB–CAA, RXB–CA and RXB–FA are shown in Fig. 9. The derived pharmacokinetic parameters for RXB alone and the three eutectics are given in Table 1. At 720 minutes the RXB concentration was below the limit of detection and, therefore, the pharmacokinetic parameters were calculated till 360 minutes.

Following a single oral dose, the maximum plasma concentration (C_{max}) of RXB is 3.14 ± 0.31 μg mL^{-1} at 55 minutes (T_{max}) after administration. The area under the curve ($AUC_{0\text{-inf}}$) of the plasma concentration *versus* time profile, which is the primary parameter indicating bioavailability, is estimated to be 536 ± 65 μg min mL^{-1}. Among the eutectics, RXB–CAA (C_{max} = 3.00 ± 0.03 μg mL^{-1}, T_{max} = 55 min) and RXB–CA (C_{max} = 2.91 ± 0.3 μg mL^{-1}, T_{max} = 55 min) showed higher $AUC_{0\text{-inf}}$ compared to pure RXB, *i.e.*, 840 ± 75 μg min mL^{-1} and 762 ± 63 μg min mL^{-1}, respectively. RXB–CAA showed a 1.5 times increase in relative bioavailability compared to the RXB standard, whereas RXB–CA showed a 1.4 times improvement. Both eutectics have comparable C_{max} and T_{max} values. In the case of RXB–FA, the pharmacokinetic parameters showed a negative trend with a decrease in C_{max} (1.27 ± 0.36 μg mL^{-1}) and $AUC_{0\text{-inf}}$ (311 ± 56 μg min mL^{-1}). Comparing the *in vitro* dissolution and *in vivo* bioavailability data, it is evident that the improvement in dissolution properties is ascribed to physiological conditions in the case of RXB–CAA and RXB–CA, whereas in the case of RXB–FA, there was a surprising decrease in bioavailability. Though RXB–FA shows a higher *in vitro* dissolution rate, it does not get absorbed into the blood effectively. This could be due to the polar nature of fumaric acid (theoretical log*P* 0.28) compared to caffeic acid and coumaric acid (theoretical log*P* 1.8 and 1.7, respectively, ESI† Table S6).

Accelerated stability study

Eutectics have high energy and high entropy due to external strain, which is the main reason for their poor stability.[7,8] Thus, assessing the stability of these eutectics is very important to obtain regulatory approval. The eutectics were subjected to the accelerated conditions of temp 40 ± 2 °C and RH 75% ± 2% for six months and the DSC thermograms of these samples were recorded.[45] After six months of stability study, the DSC thermograms recorded for all the eutectics were similar to the DSC thermograms recorded for the freshly

Table 1 Pharmacokinetic parameters for pure rivaroxaban and eutectics

Parameters	UNIT	RXB	RXB–CAA (1 : 2)	RXB–CA (1 : 2)	RXB–FA (1 : 2)
$t_{1/2}$	min	148.7 ± 35.3	133 ± 27 ns	196 ± 27 ns	130 ± 9.5 ns
T_{max}	min	55 ± 0	55 ± 0 ns	55 ± 0 ns	90 ± 0
C_{max}	μg mL^{-1}	3.14 ± 0.31	3 ± 0.03 ns	2.9 ± 0.3 ns	1.27 ± 0.36
AUC_{0-t}	μg mL^{-1} min^{-1}	427 ± 20	671 ± 14.4	520 ± 31	255 ± 54
$AUC_{0\text{-inf}}$	μg mL^{-1} min^{-1}	536 ± 65	840 ± 75	762 ± 63	311 ± 56
Volume of distribution (VD)	mL	1189 ± 146	681 ± 78	1112 ± 74 ns	1865 ± 481
Clearance (CL)	mL min^{-1}	5.64 ± 0.71	3.58 ± 0.32	3.95 ± 0.32	9.85 ± 1.81

prepared eutectics. Moreover, these thermograms did not show any additional peaks suggesting their higher stability over the tested time period under accelerated conditions (ESI† Fig. S5).

Long term stability study

The stability of the eutectics was also checked for 12 months under ambient conditions. Under ambient conditions throughout the year, the average temperature and relative humidity show a variation of 30 ± 2 °C and 60% ± 5% RH, respectively. The long-term stability of the eutectics was checked using the DSC and PXRD techniques, which revealed high stability and no change in the crystal phases upon storage for all the eutectics (ESI† Fig. S5 and S6).

Prediction of intermolecular associations using DFT studies

Using DFT, the molecular interactions in various eutectic mixtures (RXB–MA, RXB–FA, RXB–CAA, and RXB–TA) have been predicted. All the possible dimer structures of the acids have been optimized at the B3LYP/TZVP level of theory. The optimized structures of RXB, fumaric acid dimers and RXB–FA are shown in Fig. 10. The optimized structures of the other acid dimers (homosynthons) and their corresponding heterosynthons are given in the ESI† (Fig. S7 and S8). The DFT calculations revealed that the Gibbs free interaction energy (ΔG_{int}) between similar molecules (homosynthons or cohesive interactions) is greater than that of dissimilar molecules (heterosynthons or adhesive interactions) (ESI† Table S7). This is likely due to weakening van der Waals forces in the eutectic systems. This is evident from the NCI plots, representing strong attraction with blue, weak association with green, and strong repulsion with red (ESI† Fig. S9 and S10). It has been observed that homosynthons exhibit stronger attraction in the form of hydrogen bonds in all the acid dimer cases. Furthermore, in the RXB dimer case, in addition to hydrogen bonds, π–π stacking between two aromatic rings provides additional stability, as shown in the ESI† (Fig. S8 and S9). The crystal structures of RXB,[46] RXB–malonic acid[9,10] and RXB–oxalic acid[47] also revealed their dimeric structure similar to Fig. 10a (ESI† Fig. S11), thereby validating the optimized geometry. However, in contrast to the homosynthons, in the eutectic system, π–π interactions are seen to be completely absent, and only hydrogen bonding interactions dominate (Fig. 10c, ESI† Fig. S7 and S10), thereby explaining their weaker association. It is also to be noted that the eutectic system consisting of RXB–MA and RXB–CAA exhibits higher interaction energies (−5.6 and −5.5 kcal mol^{-1}, respectively) compared to RXB–FA and RXB–TA (−3.3 and −4.5 kcal mol^{-1}, respectively). This is due to the additional C–H···π interactions in RXB–MA and RXB–CAA, providing stability to such systems (ESI† Fig. S7 and S10). We have also observed that the interaction between the fumaric acid (FA) dimer and a single molecule of the drug RXB is 6.5 kcal mol^{-1} more favorable than the interaction between two molecules of RXB, as demonstrated in the ESI† (entries 10 and 11 in Table S7). These findings shed light on the experimental observation that RXB–FA is formed in a 1 : 2 ratio rather than a 1 : 1 ratio.

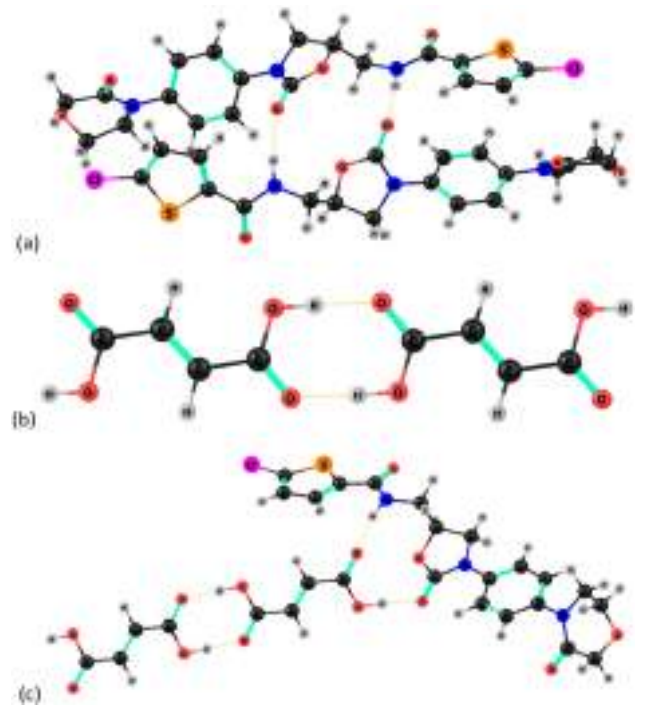

Fig. 10 Optimized structures of the RXB homosynthon (a), FA homosynthon (b) and RXB–FA heterosynthon (c).

Conclusions

In summary, we have prepared a total of six eutectics of RXB using the liquid assisted grinding method. All the eutectics were thoroughly characterized by melting point measurements, hot stage microscopy, differential scanning calorimetry, powder X-ray diffraction, and infrared spectroscopy. Melting point data, DSC thermograms, and HSM photomicrographs confirmed the formation of eutectics, whereas powder X-ray diffractograms and IR spectra revealed the reminiscence of individual components, which are characteristics of eutectics. The solubility studies revealed the enhancement in solubility for eutectics RXB–CAA, RXB–CA and RXB–FA compared to RXB alone. In contrast, eutectics RXB–SA, RXB–MA and RXB–TA showed comparable solubility with RXB. The studies on solubility and dissolution rates also revealed that the solubility and dissolution of physical mixtures of RXB with selected coformers remained similar to those of pure RXB. The solubility and dissolution rates of the physical mixtures were found to be similar to those of pure RXB. Similarly, the dissolution rate measurements revealed the enhanced cumulative release for the eutectics RXB–CAA, RXB–CA and RXB–FA compared to the RXB standard. The studies confirmed that the aqueous solubility and dissolution rate

could be enhanced by preparing API eutectics with suitable coformers.[48] The highest dissolution rate was observed for the RXB–FA eutectic followed by the RXB–CA and RXB–CAA eutectics. The present study has shown that improved *in vitro* dissolution rate of RXB–CA and RXB–CAA has translated to *in vivo* improvement in the pharmacokinetic parameters. There is a 1.5 and 1.4 times improvement in the relative bioavailability of RXB–CAA and RXB–CA, respectively, when compared with pure rivaroxaban. However, it is observed that RXB–FA showed a decrease in the pharmacokinetic parameters. The stability studies under accelerated ICH conditions for six months and the long-term stability studies for one year showed that all the eutectics were stable. The DFT studies on predicting the most favorable associations also revealed a higher possibility for homosynthons than heterosynthons, thereby supporting the formation of eutectics rather than cocrystals. We believe that the eutectics of RXB with CAA and CA may offer greater solubility, dissolution rates and bioavailability than RXB alone and can be an alternative to RXB. The preparation of eutectics of RXB with other drug components is currently being explored to achieve synergetic therapeutic efficacy. Furthermore, because of the low melting point of eutectic RXB–MA (1 : 4), efforts are being made to explore its use as a novel solid formulation for preparing amorphous solid dispersions (ASD) by employing the hot melt extrusion technique.

Author contributions

RGG conceived, designed and supervised the project. PSS and CPG performed all the experiments and data analysis. HS and KV carried out the DFT studies. KRM and SP supervised the project. SA supervised the PK studies. RGG and PSS wrote the manuscript. All the authors have approved the final version of the manuscript.

Conflicts of interest

There are no conflicts to declare.

Acknowledgements

This work was supported by the Science and Engineering Research Board, New Delhi (grant number EEQ/2018/001172). The help rendered by Mr. Tabrez Shaikh of the Physical and Materials Chemistry Division, CSIR-NCL in carrying out the DSC, PXRD, HSM, IR and dissolution studies is gratefully acknowledged. The support and the resources provided by the 'PARAM Brahma Facility' under the National Supercomputing Mission, Government of India, at the Indian Institute of Science Education and Research (IISER) Pune are gratefully acknowledged.

References

1 T. J. Milling and S. Kaatz, *Am. J. Emerg. Med.*, 2016, **34**, 39–45.
2 T. F. Thomas, V. Ganetsky and S. A. Spinler, *Clin. Ther.*, 2013, **35**, 4–27.
3 **https://www.accessdata.fda.gov/drugsatfda_docs/label/2018/022406s028lbl.pdf**.
4 A. A. Khorana, G. A. Soff, A. K. Kakkar, S. Vadhan-Raj, H. Riess, T. Wun, M. B. Streiff, D. A. Garcia, H. A. Liebman, C. P. Belani, E. M. O'Reilly, J. N. Patel, H. A. Yimer, P. Wildgoose, P. Burton, U. Vijapurkar, S. Kaul, J. Eikelboom, R. McBane, K. A. Bauer, N. M. Kuderer and G. H. Lyman, *N. Engl. J. Med.*, 2019, **380**, 720–728.
5 A. Grunenberg, J. Lenz, G. A. Braun, B. Keil and C. R. Thomas, PCT, WO2007039132 A1, 2007.
6 Z. Xie, Y. Tian, X. Lv, X. Xiao, M. Zhan, K. Cheng, S. Li and C. Liao, *Eur. J. Med. Chem.*, 2018, **146**, 299–317.
7 S. Cherukuvada and A. Nangia, *Chem. Commun.*, 2014, **50**, 906–923.
8 G. Bolla, B. Sarma and A. K. Nangia, *Chem. Rev.*, 2022, **122**, 11514–11603.
9 A. Grunenberg, K. Fähnrich, O. Queckenberg, C. Reute, B. Keil, K. S. Gushurst and E. J. Still, *US Pat.*, US20110152266 A1, 2011.
10 D. P. Kale, B. Ugale, C. M. Nagaraja, G. Dubey, P. V. Bharatam and A. K. Bansal, *Mol. Pharmaceutics*, 2019, **16**, 2980–2991.
11 É. Sipos, G. K. Lax, B. Volk, J. Barkóczy, M. Mezövári, Z. Varga and A. Dancsó, PCT, WO2013054146 A1, 2012.
12 S. Cherukuvada and T. N. Guru Row, *Cryst. Growth Des.*, 2014, **14**, 4187–4198.
13 T. Rajbongshi, K. K. Sarmah, A. Sarkar, R. Ganduri, S. Cherukuvada, T. S. Thakur and R. Thakuria, *Cryst. Growth Des.*, 2018, **18**, 6640–6651.
14 D. P. Karothu, S. Cherukuvada, L. D. Stephen and T. N. Guru Row, *CrystEngComm*, 2014, **16**, 9930–9938.
15 T. Vasconcelos, B. Sarmento and P. Costa, *Drug Discovery Today*, 2007, **12**, 1068–1075.
16 S. Emami, M. Siahi-Shadbad, M. Barzegar-Jalali and K. Adibkia, *J. Drug Delivery Sci. Technol.*, 2018, **45**, 101–109.
17 S.-M. Hyun, B. J. Lee, S. M. Abuzar, S. Lee, Y. Joo, S.-H. Hong, H. Kang, K.-A. Kwon, S. Velaga and S.-J. Hwang, *Int. J. Pharm.*, 2019, **554**, 61–71.
18 S. Singh and J. Singh, *Int. J. Pharma Bio Sci.*, 2010, **1**, 27–34.
19 M.-K. Chun, K. Hossain, S.-H. Choi, S.-J. Ban, H. Moon and H.-K. Choi, *J. Pharm. Invest.*, 2012, **42**, 139–146.
20 U. Gala, H. Pham and H. Chauhan, *J. Dev. Drugs*, 2012, **2**, 1000e130.
21 K. Chadha, M. Karan, R. Chadha, Y. Bhalla and K. Vasisht, *J. Pharm. Sci.*, 2017, **106**, 2026–2036.
22 S. R. Fukte, M. P. Wagh and S. Rawat, *Int. J. Pharm. Pharm. Sci.*, 2014, **6**, 9–14.
23 A. Araya-Sibaja, J. Vega-Baudrit, T. Guillén-Girón, M. Navarro-Hoyos and S. Cuffini, *Pharmaceutics*, 2019, **11**, 112.
24 E. L. Charsley, P. G. Laye, H. M. Markham and T. Le Goff, *Thermochim. Acta*, 2010, **497**, 72–76.
25 S. Vyazovkin, *Anal. Chem.*, 2010, **82**, 4936–4949.
26 J. Haneef and R. Chadha, *AAPS PharmSciTech*, 2017, **18**, 2279–2290.

27 *TURBOMOLE V7.5.0 2016*, a development of University of Karlsruhe and ForschungszentrumKarlsruhe GmbH, 1989–2007, TURBOMOLE GmbH, since 2007.
28 A. D. Becke, *J. Chem. Phys.*, 1993, **98**, 5648–5652.
29 C. Lee, W. Yang and R. G. Parr, *Phys. Rev. B: Condens. Matter Mater. Phys.*, 1988, **37**, 785–789.
30 S. H. Vosko, L. Wilk and M. Nusair, *Can. J. Phys.*, 1980, **58**, 1200–1211.
31 P. J. Stephens, F. J. Devlin, C. F. Chabalowski and M. J. Frisch, *J. Phys. Chem.*, 1994, **98**, 11623–11627.
32 A. Schäfer, C. Huber and R. Ahlrichs, *J. Chem. Phys.*, 1994, **100**, 5829–5835.
33 S. Grimme, J. Antony, S. Ehrlich and H. Krieg, *J. Chem. Phys.*, 2010, **132**, 154104.
34 T. Lu and F. Chen, *J. Comput. Chem.*, 2012, **33**, 580–592.
35 W. Humphrey, A. Dalke and K. Schulten, *J. Mol. Graphics*, 1996, **14**, 33–38.
36 H. Sun, Y. Li, X. Wu and G. Li, *J. Mol. Model.*, 2013, **19**, 2433–2441.
37 I. M. Vitez, A. W. Newman, M. Davidovich and C. Kiesnowski, *Thermochim. Acta*, 1998, **324**, 187–196.
38 A. Röttele, T. Thurn-Albrecht, J.-U. Sommer and G. Reiter, *Macromolecules*, 2003, **36**, 1257–1260.
39 P. Gabbott, *Principles and Applications of Thermal Analysis*, John Wiley & Sons, Ltd., 2008.
40 D. Law, W. Wang, E. A. Schmitt, Y. Qiu, S. L. Krill and J. J. Fort, *J. Pharm. Sci.*, 2003, **92**, 505–515.
41 S. Patil, V. Ujalambkar and A. Mahadik, *J. Drug Delivery Sci. Technol.*, 2017, **39**, 217–222.
42 European Medicine Agency, *Assessment report Xarelto TEP/KEP, CHMP Assess. Rep. Xarelto*, 2008, pp. 1–56.
43 **https://www.fda.gov/regulatory-information/search-fda-guidance-documents/dissolution-testing-immediate-release-solid-oral-dosage-forms**.
44 N. R. Wingert, N. O. dos Santos, S. C. Campanharo, E. S. Simon, N. M. Volpato and M. Steppe, *Drug Dev. Ind. Pharm.*, 2018, **44**, 723–728.
45 K. C. Waterman, *AAPS PharmSciTech*, 2011, **12**, 932–937.
46 J. Shen, G.-P. Tang and X.-R. Hu, *Acta Crystallogr., Sect. E: Crystallogr. Commun.*, 2018, **74**, 51–54.
47 E. Hriňová, E. Skořepová, I. Čerňa, J. Královičová, P. Kozlík, T. Křížek, J. Roušarová, P. Ryšánek, M. Šíma, O. Slanař and M. Šoóš, *Int. J. Pharm.*, 2022, **622**, 121854.
48 I. Sathisaran, J. M. Skieneh, S. Rohani and S. V. Dalvi, *J. Chem. Eng. Data*, 2018, **63**, 3652–3671.